

High-spin structure of normal-deformed bands in ^{84}Zr

R. Cardona and F. Cristancho

Departamento de Física, Universidad Nacional de Colombia, Bogotá, Colombia

S. L. Tabor, R. A. Kaye,* and G. Z. Solomon

*Department of Physics, Florida State University, Tallahassee, Florida 32306, USA*J. Döring[†]*Department of Physics, University of Notre Dame, Notre Dame, Indiana 46556, USA*

G. D. Johns

Los Alamos National Laboratory, Los Alamos, New Mexico 87545, USA

M. Devlin, F. Lerma, and D. G. Sarantites

Chemistry Department, Washington University, St. Louis, Missouri 63130, USA

I.-Y. Lee and A. O. Macchiavelli

Nuclear Science Division, Lawrence Berkeley National Laboratory, Berkeley, California 94720, USA

I. Ragnarsson

Department of Mathematical Physics, Lund Institute of Technology, S-21100 Lund, Sweden

(Received 3 December 2002; published 14 August 2003)

The reaction $^{58}\text{Ni}(^{32}\text{S}, \alpha 2p)$ at $E_{lab} = 135$ MeV was used to populate high-spin states in ^{84}Zr . The complete GAMMASPHERE and MICROBALL arrays were used to obtain clean γ - γ - γ line shapes to be analyzed by the Doppler shift attenuation method and to determine 27 lifetimes in the ground-state band and in two excited bands. Side-feeding times were also measured by comparing the line shapes gated with transitions above and below the state under study. The deduced electric quadrupole moments for the ground-state band are consistent with a very slow reduction with frequency with values ranging between 2.4(3) and 2.0(1)e b. The negative-parity bands feature also an approximate constancy of quadrupole moment with values similar to those in the ground-state band. Cranking calculations agree with this behavior in both parity bands and suggest an interpretation of the upper states in the ground-state band as part of a very slowly terminating band. Shell-dependent cranked Nilsson calculations explain a fourth γ cascade as pertaining to a noncollective structure terminating at $I = 20^+$.

DOI: 10.1103/PhysRevC.68.024303

PACS number(s): 21.10.Tg, 21.10.Ky, 27.50.+e

I. INTRODUCTION

One of the main tasks of nuclear structure research is the study of the nuclear shape, which in the case of rotational nuclei becomes a study of collective deformation. Experimental signatures of deformation can be sought in several measurable quantities: level energies, moments of inertia, or electromagnetic quadrupole transition strengths from which electric quadrupole moments can be deduced. Of these quantities, the quadrupole moments are the best suited to reflect quantitatively the deformation. However, the measurement of lifetimes, needed to determine them, demands much better statistics than needed to determine, e.g., level energies. For this reason the investigation of the transition probabilities was for a long time limited to low-spin states, a situation that has changed, since the present availability of large detector

arrays for both particles and gammas has made it possible to study the high angular momentum region for most mass numbers. Reaching higher spin states means in particular that in lifetime measurements the gate from above (GFA) technique can be used, overcoming the otherwise unavoidable uncertainties brought about with side-feeding when only gate from below (GFB) is possible. Quadrupole moments deduced in this way become very accurate and allow a more stringent test of models predicting shape evolution.

There are instances in which the gross features of the shape evolution are not difficult to understand, for example in the case of band termination. It is clear that because of the successive alignment of nucleon trajectories at higher rotational frequencies, the nucleus may evolve into an oblate or prolate “noncollective” shape. These investigations have shown very interesting facets since the exact evolution might depend on particular features of each nucleus, as is demonstrated by the fact that in the mass $A \sim 100$ bands are predicted to lower their quadrupole deformation as they approach termination [1,2] whereas in ^{62}Zn , although in fact the $B(E2)$ values are smaller with higher spin, theoretical

*Present address: Department of Chemistry and Physics, Purdue University Calumet, Hammond, Indiana 46323.

[†]Present address: GSI, 64291 Darmstadt, Germany.

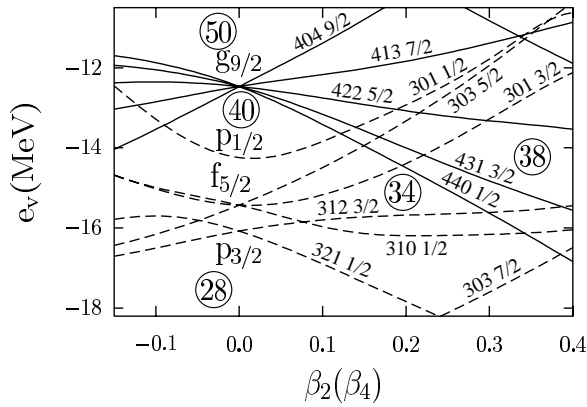


FIG. 1. Quasiparticle energies as a function of the quadrupole deformation in the $A \sim 80$ region [4].

calculations predict that the quadrupole deformation stays at about the same value within the terminating bands [3].

In the $A \sim 80$ mass region the three upper $N=3$ $p_{3/2}$, $f_{5/2}$, and $p_{1/2}$, and the lowest $N=4$ $g_{9/2}$ orbitals are the building blocks to both rotational band heads and uncoupled high-spin terminating states at medium deformation ($|\beta_2| \approx 0.2$), for both oblate and prolate shapes (see Fig. 1). The maximum spin in this valence-space configuration is $I \approx 35$, but, of course, the actual value for a given nucleus depends on the position of the Fermi level. Terminating bands at a lower value have been reported in ^{86}Zr at $I=27,30$ [5] and in ^{73}Br at $I=63/2$ [6].

Among the $A \sim 80$ nuclei, ^{84}Zr was very early identified [7] as one of the best examples of rigid rotation at high spin, i.e., one in which the moment of inertia does not change with rotational frequency. This fact attracted theoretical as well as experimental research on this nucleus. Woods-Saxon Strutinsky-Bogolyubov cranking model calculations [8] predicted the frequency and nature of the crossing in the ground-state band, whose experimental verification came later with the measurement of g factors up to the first crossing [9]. The same calculations also predicted the occurrence of superdeformed bands at very high spins, which have also been observed [10]. Lifetime measurements were carried out using the recoil distance and Doppler-shift attenuation methods (DSAM) [7,9,11] providing values in the ground-state band for states below $I^\pi=22^+$ and in two of the lowest negative parity states. Additional measurements on the level scheme and further analysis were also done [12–14], as well as renewed g -factor measurements below the first bandcrossing [15].

The above mentioned importance of electric quadrupole measurements makes very interesting investigation in the high-spin states of a nucleus such as ^{84}Zr , which are in fact the main goal of this work. Using the GFA technique, we measured the lifetimes of almost all the known normally deformed states in ^{84}Zr .

II. EXPERIMENTAL PROCEDURE AND CHANNEL SELECTION

With beams from the 88-Inch Cyclotron at Lawrence Berkeley National Laboratory, high-spin states in ^{84}Zr were

populated using the fusion-evaporation reaction $^{58}\text{Ni}(^{32}\text{S}, \alpha 2p)$ at 135 MeV and a beam intensity of 3.5 particle nA. The recoil velocity of the reaction products was $\beta = v/c \approx 0.035$. The experiment, optimized for lifetime measurements using the Doppler-shift attenuation method, made use of a $415 \mu\text{g}/\text{cm}^2$ thick ^{58}Ni target which was evaporated on a $10.3 \text{ mg}/\text{cm}^2$ Ta backing used as the stopping material for the recoiling nuclei.

The GAMMASPHERE [16] array with 95 high efficiency Ge detectors was used to collect prompt coincidence events. The evaporated charged particles were detected and identified with the MICROBALL [17] array. This array consists of 95 CsI(Tl) scintillators covering 97% of the full sphere around the target. During the experiment, a fourfold or higher γ -multiplicity trigger condition was used. Of the total number of events, 10% were associated with ^{84}Zr .

The collected data were sorted into different 3000×3000 channel square matrices. To obtain optimum selection of ^{84}Zr events, all matrices were gated on the requirement of one or two protons and one α particle detected in the MICROBALL. Nondetection of one particle can produce contamination especially coming from the four-particle channels $3p1\alpha$ (^{83}Y) and $2p2\alpha$ (^{80}Sr). Given that detection efficiencies for protons and α 's are about equal (84%) for the MICROBALL, the intensity of the leak-through γ 's finally depends also on the relative evaporation cross sections. In this case, to remove contamination from the stronger ^{83}Y channel (^{80}Sr appeared clearly weaker), 1.6 times the corresponding $3p1\alpha$ gated matrices were subtracted.

The matrices were also gated on the requirement of an additional γ ray. To select the ground-state band, this additional γ ray was required to be one of the following lines within the strongest (positive-parity) populated band: 540.0, 723.0, 873.2, 952.0, 979.2, or 1067.1 keV. The higher energy lines are broader, so the possibilities of overlapping peaks are increased. Separate matrices were sorted to enhance the negative-parity bands by requiring either the 488, 540.0, 668.2, 723.0, 832.1, 873.2, 885.1, 915.6, 1290.2, 1357.1, or 1562.1 keV lines as the additional coincident γ ray.

Gamma rays detected in any of the detectors were sorted onto one axis of the square arrays to allow for a second γ gate in selecting the line shapes. Only lines from detectors at approximately the same θ angle were sorted onto the second axis, from which the line shapes to be fitted were obtained. The following pairs of detector rings were combined: 31.72° with 37.38° , 50.07° with 58.28° , 121.72° with 129.93° , and 142.62° with 148.28° . These combinations yield weighted average angles of 34.95° (seven active detectors) 52.81° (15 active detectors), 127.19° (15 active detectors), and 145.45° (ten active detectors), respectively.

With these sorted data it was possible to create spectra by adding up many gates set on ^{84}Zr transitions. These projected spectra provided line shapes for the determination of lifetimes. Examples of such line shapes in the case of band 1 at forward and backward angles are shown in Fig. 2. Bands 2 and 3 present similar Doppler shifts. For the transitions in band 4, on the contrary, no shift was observed, as it is shown in Fig. 2(b) in the case of the 1224-keV transition.

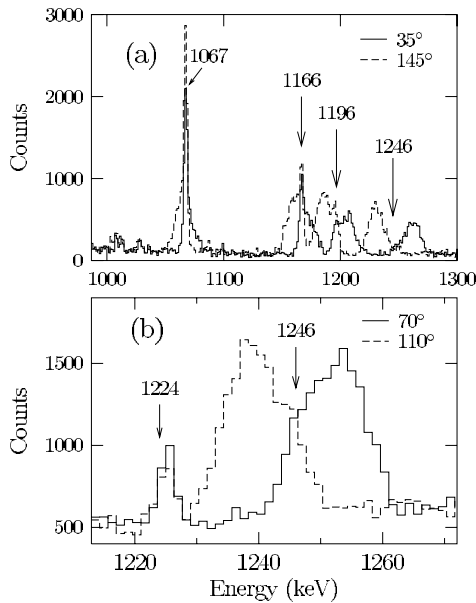


FIG. 2. (a) Comparison of forward (34.95°) and backward (145.45°) angle spectra generated by adding positive-parity high-spin gates: 1432, 1645, 1845, 1995, 2146 keV. (b) Comparison of forward (70°) and backward (110°) angle spectra to demonstrate that no Doppler-shift appears for the 1224-keV transition in band 4. The 1246-keV transition belongs to band 1. The arrows show the expected positions of the unshifted peaks.

III. LIFETIME MEASUREMENTS

Mean lifetimes for the shorter-lived higher-lying states in all bands 1 to 3 were analyzed by applying the DSAM to the experimental line shapes. The analysis carried out in the present work, using the computer code FITS [18], exactly follows the procedure described in previous reports [19,20] on data from the same experiment.

The theoretical line shapes generated by FITS for a range of possible mean lifetimes were compared to the coincidence spectra at each of the four angles, 34.95° , 52.81° , 127.19° , and 145.45° . The best fits provided lifetime values that were found to be consistent within uncertainties. The weighted average (based on the number of detectors) of the lifetimes resulting from the best individual fits was taken as the accepted lifetime at each average angle.

Except for the two highest transitions in each band, each line shape was fitted taking into account side and direct feeding from the upper levels. Side-feeding times were determined by fitting line shapes obtained GFA the transition of interest to eliminate the contribution of side-feeding. The lifetimes, determined separately at each angle, were then held fixed in fitting the same line shapes GFB. Only the side-feeding lifetimes were allowed to vary until the best fits were obtained. This is a very important characteristic of the method: side-feeding and lifetime are determined independently, a fact to take into account when comparing with results from other methods. An example of GFA and GFB line shapes is given in Fig. 3 in the case of the 1196.2-keV transition. The side-feeding times determined were then compared with the effective lifetimes of the states immediately above. Although there is some dispersion, due mainly to sta-

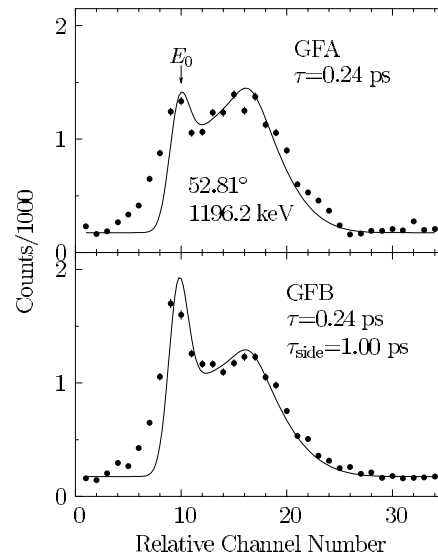


FIG. 3. The comparison of the 1196.2-keV transition at 52.81° GFA and GFB. Observe the dramatic effect of the long-lived side-feeding that strongly populates the lower spectrum (GFB) when the nuclei have already stopped ($E_\gamma \approx E_0$). Unless otherwise noted, the calibration is 1.33 keV/channel on the line shape graphs. The gates used are for GFA: 2477, 2146, 1995, 1845, 1165.8 and 1432.0 keV transitions; for GFB: 1165.8 keV line.

tistical variations, the side-feeding times averaged about 1.2 times the effective lifetime above. This average was adopted for the fits of lines which could only be gated from below.

The procedure to make gates with very low intensity lines is based on the following reasoning. The ^{84}Zr nuclei initially are produced with a recoil velocity of $v \approx 0.035c$, which is reduced to zero by collisions with electrons and atoms of the thick backing material. Thus a Doppler-broadened line extending between E_0 (energy of the γ rays emitted by a nucleus at rest) and some value $E_0 + \Delta$ is observed in the γ spectrum, whose shape depends on the relationship between lifetime and stopping time and also on the angular position of the detector. A very short lived state ($\tau < 0.02$ ps) mainly decays at the beginning of the stopping process when all the nuclei are moving at the same velocity. In this way, it is possible to correct the Doppler effect and find the expected position of the unshifted peak. When building the matrix, every γ energy is corrected according to a proposed β value and its angle of detection. Figure 4 shows the effect of this procedure in an extended γ -energy region when recovering back the peaks.

IV. RESULTS

A. Level scheme of ^{84}Zr , band 4

Figure 5 shows a summary of the high-spin bands in ^{84}Zr as observed in previous investigations [7,12,10,13,14], complemented by the results of the present study. Some known medium- and low-spin states, omitted in the figure since they are not relevant in this study, are thoroughly analyzed in Ref. [14]. The present study confirms the previously published high-spin level scheme and has allowed the extension of band 4 by two transitions.

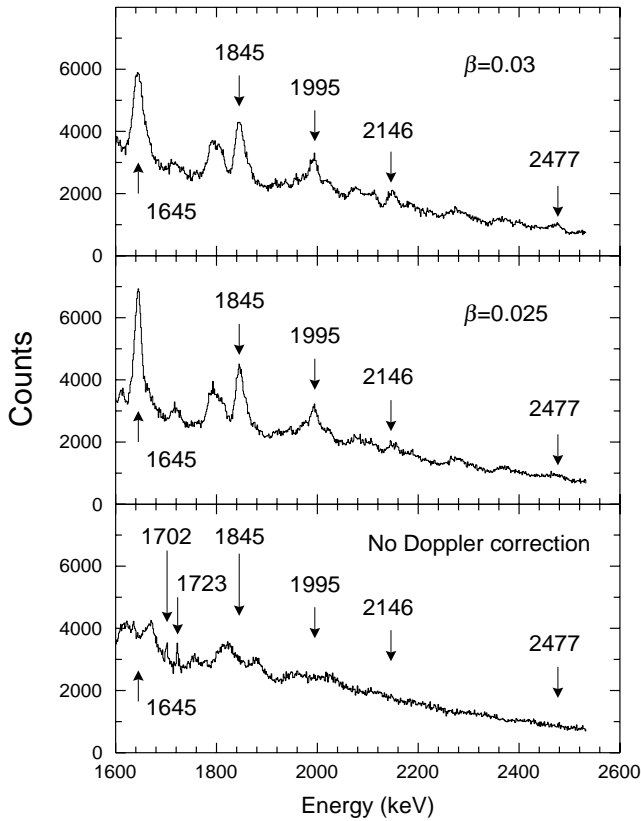


FIG. 4. Comparison of spectra with Doppler correction of $\beta=0.03$ (top), $\beta=0.025$ (middle), and no Doppler correction (bottom). A coincidence matrix with all detectors in the y axis and the detectors at 34.95° in the x axis was made. The spectra shown are the projection on the y axis. For the transitions with very short lifetimes (2477, 2146, and 1995 keV), the spectra with $\beta=0.03$ were taken to make gates. For transitions with longer lifetimes (1845 and 1645 keV), the spectra with $\beta=0.025$ were used instead because the lines are narrower. In the bottom panel, with no correction, the ground-state transitions show very wide line shapes. However, the unshifted 1702- and 1723-keV transitions of band 4 can be seen clearly.

B. DSAM Analysis

Line shapes were extracted for as many transitions and angles as possible to measure the lifetimes with the DSAM. All lifetimes measured in the present work refer to bands 1–3 and are listed in Table I. Surprisingly, the γ transitions in band 4 show sharp line shapes up to the highest observed level [see Figs. 2(b) and 4] which indicate less collectivity. The effective lifetimes are the average of values obtained at the various angles at which lifetimes could be measured.

The line shapes of the 1645.3-keV transition in band 1 are shown at all four average angles in Fig. 6 as an example of the variation with angle. Figure 7 illustrates the variation of the line shapes from a short one to that of the longest lifetimes measured.

In most cases it was possible to fit each transition individually, without interference from other peaks, by a judicious choice of gates. Where this was not possible, a modified version of FITS was used to fit two overlapping line shapes simultaneously, by comparison with the properly

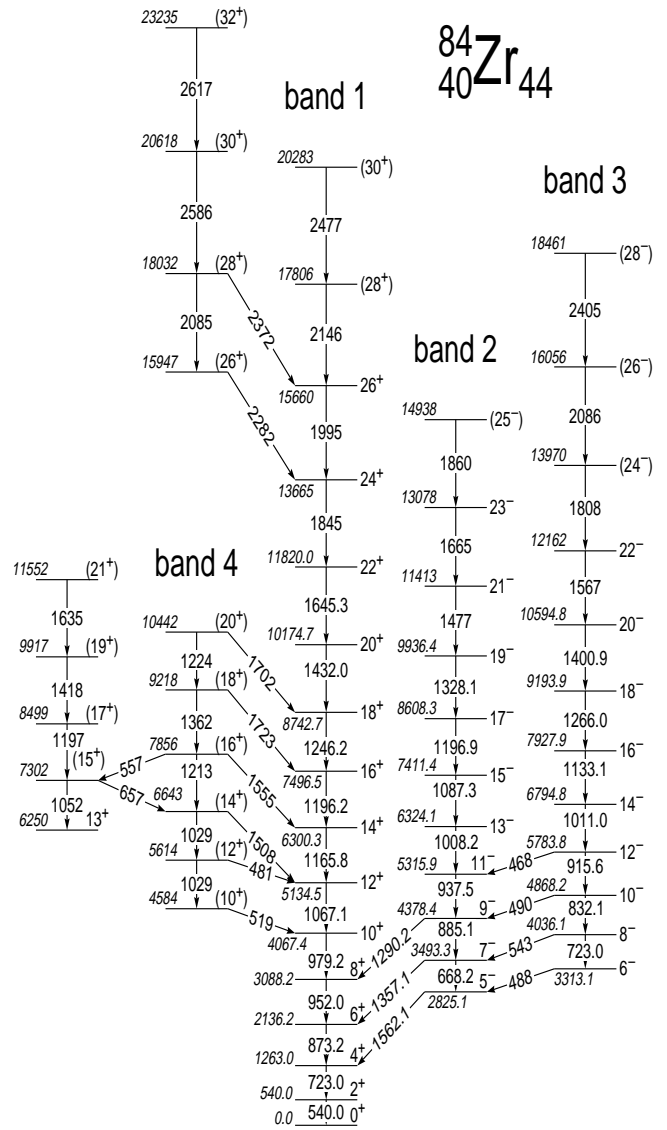


FIG. 5. Partial level scheme of ^{84}Zr based on the present study and previous work [7,12,10,13,14]. A few low- and medium-spin states have been omitted. The energies for γ transitions in bands 1–3 have been adopted from Refs. [10,13].

scaled sum of the two theoretical line shapes. This procedure was carried out to find the lifetimes of the states $I^\pi=23^-$ in band 2 and $I^\pi=(24^-)$ in band 3 whose transitions overlap with transitions at 1663 and 1808 keV, respectively, of the superdeformed band. In each case a very short lifetime ($\tau_{SD} < 0.001$ ps) [10] was assumed for the state in the superdeformed band.

A comparison between state and feeding times found in the present work and Refs. [7,9,11] for the ground-state band of ^{84}Zr is shown in Table II. With the exception of two states ($I^\pi=10^+, 20^+$), there is agreement between the previously reported lifetimes. There is also agreement between the values obtained in this work and the previously reported ones for states $I \geq 16$. However, a striking difference is observed for lifetimes of states with $I \leq 14$. Ours are 2.2–3.5 times shorter than those in Ref. [11]. This is a big difference and

TABLE I. Energies, initial spins of the states, γ -ray energies, effective lifetimes, mean lifetimes, and accepted lifetimes in ^{84}Zr . Effective and accepted lifetimes are the average of all possible angles. The GFA technique has been used for all except for the two upper transitions of each band. Energies and spin assignments were taken from Ref. [10].

E_x (keV)	I_i^π	E_γ (keV)	τ_{eff} (ps)	τ_{acc} (ps)
Band 1				
20283	(30 ⁺)	2477	0.047(14)	0.047(14)
17806	(28 ⁺)	2146	0.057(14)	0.014(11)
15660	26 ⁺	1995	0.087(18)	0.028(13)
13665	24 ⁺	1845	0.125(18)	0.019(13)
11820.0	22 ⁺	1645.3	0.176(13)	0.044(10)
10174.7	20 ⁺	1432.0	0.282(12)	0.092(11)
8742.7	18 ⁺	1246.2	0.494(18)	0.189(16)
7496.5	16 ⁺	1196.2	0.97(3)	0.240(22)
6300.3	14 ⁺	1165.8	1.61(7)	0.226(21)
5134.5	12 ⁺	1067.1	2.93(16)	0.358(32)
4067.4	10 ⁺	979.2	6.9(6)	0.517(48)
3088.2	8 ⁺	952.0	> 7	0.56(10)
Band 2				
14938	(25 ⁻)	1860	0.121(29)	0.121(29)
13078	23 ⁻	1665	0.195(28)	0.064(23)
11413	21 ⁻	1477	0.385(82)	0.131(55)
9936.4	19 ⁻	1328.1	0.79(13)	0.215(56)
8608.3	17 ⁻	1196.9	1.07(18)	0.232(78)
7411.4	15 ⁻	1087.3	1.91(43)	0.43(11)
6324.1	13 ⁻	1008.2	3.5(10)	0.66(14)
Band 3				
18461	(28 ⁻)	2405	0.081(20)	0.081(20)
16056	(26 ⁻)	2086	0.14(4)	0.03(3)
13970	(24 ⁻)	1808	0.187(28)	0.030(25)
12162	22 ⁻	1567	0.284(53)	0.056(23)
10594.8	20 ⁻	1400.9	0.319(43)	0.084(25)
9193.9	18 ⁻	1266.0	0.523(39)	0.154(33)
7927.9	16 ⁻	1133.1	1.11(60)	0.334(28)
6794.8	14 ⁻	1011.0	3.4(2)	0.73(11)

deserves a closer examination. A related issue always to be considered when evaluating state lifetimes is that of side-feeding times: although the information provided in Ref. [11] is not very precise, it is clear that our feeding times are ~ 5 – 10 times longer than in Ref. [11] and 1–2 orders of magnitude larger compared to those of Ref. [9]. These enormous differences do not seem to be accounted for only by the difference in the position of the entry states produced by each reaction, which in fact may have a sizeable effect on the length of the γ cascades but account for only small differences in feeding time. It is, however, not straightforward to compare our values with those obtained before, since although all of them have the DSA method in common, there are outstanding differences in statistics and in the method used to obtain τ_F . In this respect it is important to stress that our lifetime measurements are insensitive to the side-feeding, since the GFA technique eliminates its contribution in the line shape of the analyzed transition.

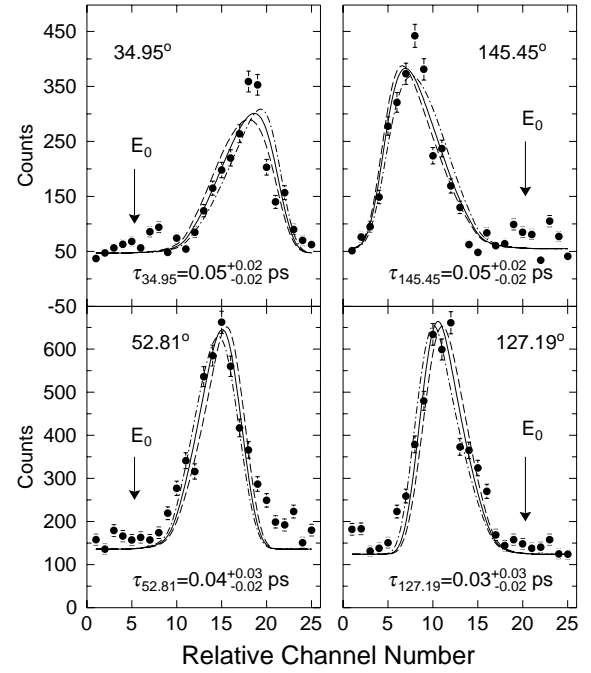


FIG. 6. The 1645.3-keV transition in band 1 fitted individually at all four angles. Fits representing the uncertainty limits are shown with dashed and dashed-dotted lines. The expected position of an unshifted 1645.3-keV line is indicated with an arrow.

In an effort to further understand the differences in side-feeding and lifetimes mentioned above, we analyzed some of the transitions in the ground-state band following a method customarily used when there is no possibility of following the “gate from above” method, i.e., when one has only the opportunity of gating below the transition studied [21]. In this kind of analysis the feeding time is kept fixed while the lifetime is fitted. By varying τ_F over a given range one obtains a correlation between this value and τ . From the minimum of the reduced χ^2 , it is then possible to extract values for both side-feeding and lifetimes. The resulting values for the analyzed lines are listed in the two last columns of Table II. The two values for the 1432.0- and 1246.2-keV transitions come about because their χ^2 plots have two minima, as can be seen in Fig. 8 for the 1432.0-keV case, one with a short side-feeding and long lifetime and the other minimum with their relative length interchanged. The “correlation” method does not provide a way to decide between short or long side-feeding and one has then to rely, for example, on systematics and/or model calculations, as was done in Ref. [22], where two-minima correlation plots in the DSAM investigation of ^{83}Y were also obtained. One can even decide to take the shorter side-feeding, as was believed for a long time, because of the lack of convincing experimental arguments on long side-feeding times. The conclusion from Table II is twofold: on one hand it shows the weakness of the correlation method that may lead to not well justified short side-feeding times (and longer lifetimes); and on the other hand, the same method supports the long side-feeding times and shorter lifetimes produced by the GFA method, since besides those fits in which only one minimum is found, $I^\pi = 12^+ - 16^+$, in

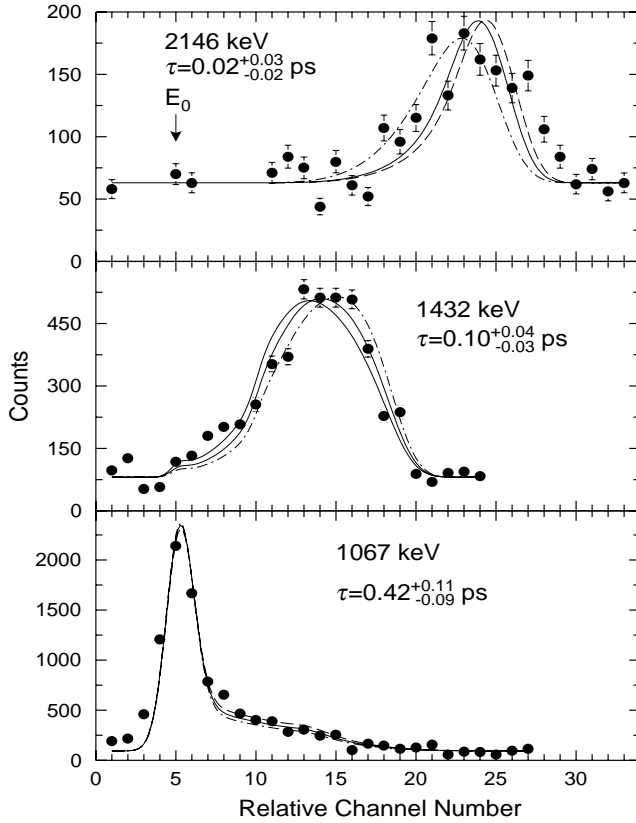


FIG. 7. Typical fits at 34.95° taken from band 1 to illustrate the sensitivity of the line shape to the state lifetime. The calibration for the 2146 and 1432 keV graphs is 2.67 keV/channel.

which case the correlation results are very similar to the GFA ones, also the upper minimum of the double-minima fits produce τ and τ_F similar in both methods.

Another eventual origin for differences in results from DSAM lifetime measurements is the modeling of the stopping power, which may not be the case in the present comparisons since Refs. [11,9] quote the use of the Ziegler-Biersack-Littmark parametrization [23], a predecessor to the computer code SRIM [24] used in the present work. There are in the literature other stopping power functions which however, have proved [25] not to be as adequate as the parametrization ZBL.

Considering the values obtained in the present work (Table II), it is important to note that the side-feeding times are much larger than the state lifetimes. A graphical way to convince ourselves of this fact is to observe the dramatic increase in the “stop-peak” (slow feeding intensity) when gating from below as compared to when gating from above (no side-feeding) in Fig. 3. The ratio $\langle \tau_F / \tau \rangle$ for states $12 \leq I \leq 20$ averages to ≈ 3.6 , which compares well with $\langle \tau_F / \tau \rangle \approx 3.4$ measured in the ground-state band of ^{82}Sr [26]. The highest state in which feeding time was measured ($I = 26$) has a ratio of 2.9, consistent with the average, whereas the ratio for the state $I = 24$ is the largest one with $\langle \tau_F / \tau \rangle = 7.4$. The large error bars of the side-feeding and lifetimes for this state make, however, the latter value less certain. A recent version of the Monte Carlo code GAMMAPACE [27,28]

was used to investigate the possible origin of these long side-feeding times. In order to obtain the observed values in ^{84}Zr , it is necessary to assume that the continuum decay is dominated by slowly decaying single-particle structures in contrast with the fast collective decaying states assumed [21,28] in other nuclei in this mass region. Although one could relate this result with a probable transitional character of ^{84}Zr in the continuum states, there is no obvious interpretation for these side-feeding time results and additional experimental and theoretical investigations are needed.

C. Transition strengths and quadrupole moments

The electric quadrupole transition strengths $B(E2)$ were determined from the accepted lifetimes and transition energies given in Tables I and II by means of

$$B(E2; I \rightarrow I-2) [e^2 b^2] = \frac{0.0816}{E_\gamma^5 [\text{MeV}] \tau [\text{ps}]} \quad (1)$$

If an axially symmetric nucleus is supposed, the rotational model gives a simple relationship between quadrupole moment and reduced transition strengths,

$$B(E2, I \rightarrow I-2) = \frac{5}{16\pi} \langle IK20 | I-2K \rangle^2 Q_t^2, \quad (2)$$

where $\langle IK20 | I-2K \rangle$ is a Clebsch-Gordan coefficient. A value of $K=0$ was used for band 1. The choice of K for the negative-parity bands deserves a short discussion: putting aside K mixing, with the present experimental knowledge it is only possible to state that $K \leq 5$. Since we are dealing with high spins, $I \geq 13$, no essential differences appear regarding the $|Q_t|$ values for $K=3, 4$, or 5. Assuming the proton character of these bands as given by the positive g factor [9], the lowest excited configurations (see Fig. 1) have $K=5$ at small oblate deformation and $K=4$ at the prolate side. Since the negative-parity bands are strongly Coriolis mixed, an “effective” K results from a weighted average. $K=4$ seems to be a representative value.

Quadrupole deformation β_2 and triaxiality γ are related to the transition quadrupole moment by [29]

$$Q_t = \frac{6ZeA^{2/3}}{(15\pi)^{1/2}} r_0^2 \beta_2 (1 + 0.36\beta_2) \cos(30^\circ + \gamma). \quad (3)$$

The quantities $B(E2)$, the transition quadrupole moments $|Q_t|$, and the deformation β_2 (assuming $\gamma=0^\circ$ and $r_0 = 1.2$ fm) are given in Table III.

Given the observed differences in the lifetimes between our results and the previously reported ones for the ground-state band, it is important to compare their implications regarding transition quadrupole moments. Figure 9 compares those results and shows also the values for those spins not measured in this work. It is now clear that the difference in lifetimes leads to very different conclusions about the structure of ^{84}Zr . The most striking feature in our results is the apparent constancy of the quadrupole moments over a wide range of spin and the big difference for $I \leq 14$ with the entire

TABLE II. Summary of state and side-feeding times for the rotational bands of ^{84}Zr . In the present work, lifetime determination independent of side-feeding effects (GFA technique) has been used for all except for the two upper transitions. The values under ‘‘correlation’’ result from an analysis (see text) in which no GFA is used.

E_x (keV)	I_i^π	E_γ (keV)	τ^a	τ^b	τ_F^b	τ^c	τ_F (ps) ^c	GFA		Correlation	
								τ^d	τ_F^d	τ^d	τ_F^d
20283	(30 ⁺)	2477						0.047(14)			
17806	(28 ⁺)	2146						0.014(11)			
15660	26 ⁺	1995						0.028(13)	0.08(3)		
13665	24 ⁺	1845						0.019(13)	0.14(5)		
11820.0	22 ⁺	1645.3	0.02(1)			0.05(2)	0.08	0.044(10)			
10174.7	20 ⁺	1432.0	0.03(1)			0.10(5)	0.04-0.12	0.092(11)	0.23(3)	0.09(2)	0.24(5)
										0.15(2)	0.06(3)
8742.7	18 ⁺	1246.2	0.16(1)			0.17(6)	0.04-0.12	0.189(16)	0.31(6)	0.16(2)	0.42(13)
										0.22(2)	0.13(8)
7496.5	16 ⁺	1196.2	0.18(2)	0.18	0.01	0.21(7)	0.04-0.12	0.240(22)	1.0(2)	0.28(5)	0.8(5)
6300.3	14 ⁺	1165.8	0.50(5)	0.49(3)	0.04	0.6(2)	0.12	0.226(21)	1.0(1)	0.19(2)	1.4(4)
5134.5	12 ⁺	1067.1	0.9(2)	0.87(4)	0.20	0.8(2)	0.16	0.358(32)	1.9(3)	0.40(5)	1.4(4)
4067.4	10 ⁺	979.2	1.5(3)	0.77(5)	0.24	1.4(3)	0.28	0.517(48)			
3088.2	8 ⁺	952.0	2.0(5)	1.8(1)	0.22	2.1(5)	0.42	0.56(10)			
2136.2	6 ⁺	873.2	2.6(4)								
1263.0	4 ⁺	723.0	4.0(6) ^e								
540.0	2 ⁺	540.0	20.3(11) ^e			24(2) ^e					
3493.3	7 ⁻	668.2	7.8(30) ^e								
2825.1	5 ⁻	1562.1	15.7(50) ^e								

^a $^{58}\text{Ni}(^{28}\text{Si},2p)$, $^{58}\text{Ni}(^{29}\text{Si},2pn)$ $E_{lab}=95-110$ MeV, Ref. [7].

^b $^{54}\text{Fe}(^{33}\text{S},2pn)$ $E_{lab}=105$ MeV, Ref. [9].

^c $^{59}\text{Co}(^{28}\text{Si},p2n)$ $E_{lab}=98$ MeV, Ref. [11].

^d $^{58}\text{Ni}(^{32}\text{S},\alpha2p)$ $E_{lab}=135$ MeV, present work.

^eRecoil-distance method.

set of the previous measurements. The reason for these differences seems to be in the different treatment of side-feeding time as discussed in Sec. IV B.

V. DISCUSSION

In rotational nuclei the most frequent microscopic change of configuration means the breaking of a pair, which according to a simple interpretation implies (i) that two nucleons do

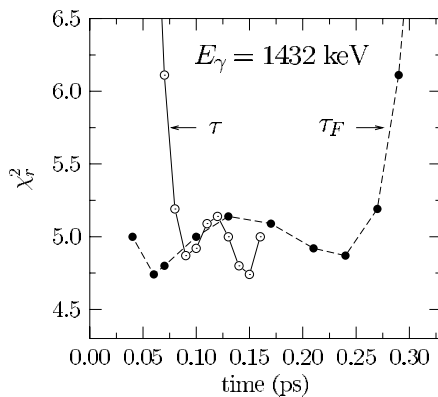


FIG. 8. Correlation plot for the 1432-keV transition as produced when fitting both τ_F and τ simultaneously. This plot produces two pairs of acceptable values: $(\tau, \tau_F) = (0.09, 0.24)$ and $(0.15, 0.06)$ ps.

not participate any more in the collective core movement, and that (ii) besides contributing to the shaping of the entire nucleus through the geometrical position of their orbitals, the new valence nucleons can exert polarizing forces on the remaining core. Both effects may cause the collective shape and therefore $|Q_i|$ to change in some amount. Although the exact microscopic mechanism depends, of course, on the details of the configuration, the appearance of such effects can be detected by examining quantities such as the kinematic and dynamic moments of inertia together with the quadrupole moment. In the following section we will give first a description of the three collective bands, relating them to previously existing theoretical analyses [8]. These calculations considered pairing only at $\omega=0$ and therefore strict correlations with shape parameters cannot be stated in this section, but they are still useful in helping to distinguish the interplaying configurations. Then we will study the results regarding quadrupole moments in the light of new theoretical calculations including pairing and, therefore, allowing correct predictions on deformation parameters. Finally we will offer an explanation of the origin of the noncollective band 4.

A. Cranking analysis

The moments of inertia, kinematic $\mathcal{J}^{(1)}$ and dynamic $\mathcal{J}^{(2)}$, together with the electric quadrupole transition mo-

TABLE III. Excitation energies, initial spins, transition energies, electric transition quadrupole strengths, electric transition quadrupole moments, and quadrupole deformation (assuming $\gamma=0^\circ$) for states in rotational bands of ^{84}Zr . Every transition is stretched quadrupolar ($\Delta I=2$), therefore only initial spin is given. Note that all but the two upper transitions in each band were analyzed with the GFA technique.

E_x (keV)	$I_i^\pi(\hbar)$	E_γ (keV)	$B(E2)$ (W.u.) ^a	$ Q_t $ (eb)	β_2
Band 1					
20283	(30 ⁺)	2477	9_{-2}^{+4} b	$0.72^{+0.14}_{-0.09}$ b	$0.08^{+0.02}_{-0.01}$ b
17806	(28 ⁺)	2146	59_{-26}^{+215} c	$1.89^{+2.19}_{-0.48}$ c	$0.21^{+0.21}_{-0.05}$ c
15660	26 ⁺	1995	42_{-13}^{+37}	$1.60^{+0.59}_{-0.28}$	$0.18^{+0.06}_{-0.03}$
13665	24 ⁺	1845	92_{-37}^{+199}	$2.37^{+1.85}_{-0.54}$	$0.26^{+0.18}_{-0.06}$
11820.0	22 ⁺	1645.3	70_{-13}^{+21}	$2.08^{+0.29}_{-0.20}$	$0.23^{+0.03}_{-0.02}$
10174.7	20 ⁺	1432.0	67_{-7}^{+9}	$2.04^{+0.13}_{-0.11}$	$0.23^{+0.01}_{-0.01}$
8742.7	18 ⁺	1246.2	66_{-5}^{+6}	$2.02^{+0.09}_{-0.08}$	$0.22^{+0.01}_{-0.01}$
7496.5	16 ⁺	1196.2	64_{-5}^{+6}	$1.99^{+0.10}_{-0.09}$	$0.22^{+0.01}_{-0.01}$
6300.3	14 ⁺	1165.8	77_{-6}^{+8}	$2.20^{+0.11}_{-0.10}$	$0.24^{+0.01}_{-0.01}$
5134.5	12 ⁺	1067.1	76_{-6}^{+7}	$2.20^{+0.11}_{-0.09}$	$0.24^{+0.01}_{-0.01}$
4067.4	10 ⁺	979.2	80_{-7}^{+8}	$2.28^{+0.11}_{-0.10}$	$0.25^{+0.01}_{-0.01}$
3088.2	8 ⁺	952.0	85_{-13}^{+18}	$2.39^{+0.25}_{-0.19}$	$0.26^{+0.02}_{-0.02}$
Band 2					
14938	(25 ⁻)	1860	14_{-3}^{+4} b	$0.94^{+0.14}_{-0.10}$ b	$0.11^{+0.02}_{-0.01}$ b
13078	23 ⁻	1665	46_{-12}^{+26} c	$1.73^{+0.43}_{-0.25}$ c	$0.19^{+0.04}_{-0.03}$ c
11413	21 ⁻	1477	41_{-12}^{+29}	$1.64^{+0.51}_{-0.26}$	$0.18^{+0.05}_{-0.03}$
9936.4	19 ⁻	1328.1	42_{-9}^{+15}	$1.69^{+0.28}_{-0.19}$	$0.19^{+0.03}_{-0.02}$
8608.3	17 ⁻	1196.9	66_{-16}^{+33}	$2.15^{+0.49}_{-0.29}$	$0.24^{+0.05}_{-0.03}$
7411.4	15 ⁻	1087.3	57_{-12}^{+20}	$2.05^{+0.33}_{-0.22}$	$0.23^{+0.03}_{-0.02}$
6324.1	13 ⁻	1008.2	54_{-10}^{+15}	$2.07^{+0.26}_{-0.19}$	$0.23^{+0.03}_{-0.02}$
Band 3					
18461	(28 ⁻)	2405	6_{-1}^{+2} b	$0.60^{+0.09}_{-0.06}$ b	$0.07^{+0.01}_{-0.01}$ b
16056	(26 ⁻)	2086	$32_{-16}^{+\infty}$ c	$1.42^{+\infty}_{-0.42}$ c	$0.16^{+\infty}_{-0.05}$ c
13970	(24 ⁻)	1808	64_{-29}^{+322}	$2.04^{+2.96}_{-0.53}$	$0.23^{+0.28}_{-0.06}$
12162	22 ⁻	1567	71_{-20}^{+49}	$2.16^{+0.65}_{-0.34}$	$0.24^{+0.07}_{-0.04}$
10594.8	20 ⁻	1400.9	82_{-19}^{+35}	$2.35^{+0.46}_{-0.29}$	$0.26^{+0.05}_{-0.03}$
9193.9	18 ⁻	1266.0	75_{-13}^{+20}	$2.27^{+0.29}_{-0.21}$	$0.25^{+0.03}_{-0.02}$
7927.9	16 ⁻	1133.1	60_{-5}^{+5}	$2.07^{+0.09}_{-0.08}$	$0.23^{+0.01}_{-0.01}$
6794.8	14 ⁻	1011.0	49_{-6}^{+9}	$1.92^{+0.16}_{-0.13}$	$0.21^{+0.02}_{-0.01}$

^a1 W.u. = $21.9 e^2 \text{ fm}^4$.

^bValue extracted from effective lifetime.

^cLifetime determined from gate from below only.

ment $|Q_t|$ are plotted for the three collective bands of ^{84}Zr in Fig. 10. It is convenient to analyze separately the ground-state and the excited, negative-parity bands.

1. Ground-state band

Figure 10 displays strong variations in $\mathcal{J}^{(1)}$ at low frequency which reflect themselves in “peaks” in $\mathcal{J}^{(2)}$ indicating band crossings that have been successfully explained by Woods-Saxon cranking [8] calculations. They correctly predict both crossings as caused by first a $g_{9/2}$ proton alignment and second a $g_{9/2}$ neutron alignment. The first alignment was confirmed experimentally by a g factor measurement [9].

The general trend of $|Q_t|$ can be considered as a very slow decrease in the frequency range measured in the present

work. In fact, the eight lower values, corresponding to states at frequencies $0.48 \leq \hbar\omega \leq 0.82$ MeV have small enough error bars to allow the observation of a reduction of only 13% between these two extreme frequencies. The higher-spin state at $\hbar\omega \approx 1$ MeV, with also a relatively small error bar, indicates that if the quadrupole moment diminishes at higher frequencies, such a reduction is not drastic. The two other values at $\hbar\omega \approx 0.92, 1.07$ MeV, although with extended error bars in the large quadrupole moment side, are consistent with either a constant value or with a very slight reduction at higher frequencies. The last point at $\hbar\omega \approx 1.24$ MeV, as the other data enclosed in square brackets, having been extracted from an effective lifetime, gives only a lower limit and therefore cannot be used as information about the $|Q_t|$'s trend. It is worth noting that the frequency region measured starts

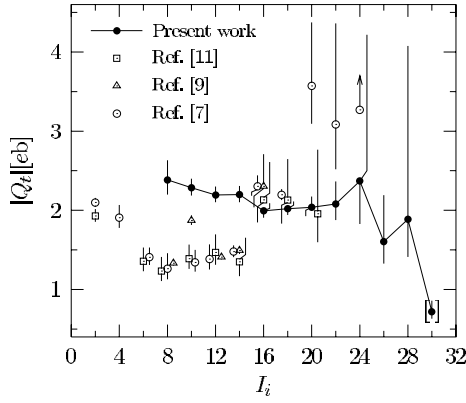


FIG. 9. Comparison between the transition quadrupole moments found in the present work and the previously reported ones for the ground-state band [11,9,7]. The value enclosed in square brackets ($I=30$) is extracted from the effective lifetime and means therefore a lower limit. Some of the values have been slightly shifted backward or forward around the corresponding spin in order to appreciate their relative errors. $|Q_t|(I=2,4)$ were obtained from recoil-distance method measurements, all others from DSAM.

while the first alignment is taking place and that the change in $|Q_t|$ during the whole alignment process is only 8%, whereas in the same region the kinematic moment of inertia $\mathcal{J}^{(1)}$ changes by $\approx 80\%$ of the initial value. The data indicate that the first two alignments do not drastically alter the deformation or collectivity of this nucleus, a conclusion supported by the theoretical predictions presented in the following section. This behavior is in marked contrast with ^{74}Kr , in which a drastic lowering in $|Q_t|$, explained too by

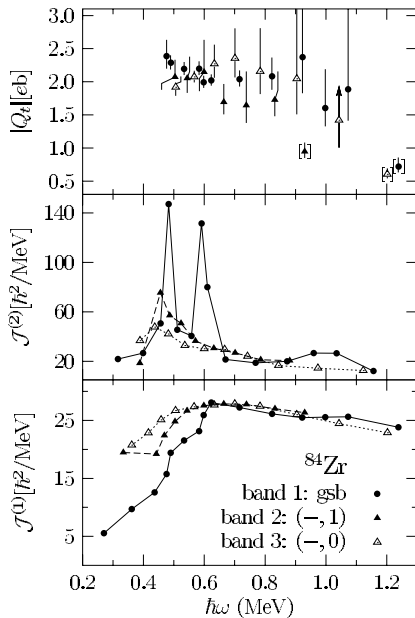


FIG. 10. Kinematic $\mathcal{J}^{(1)}$ and dynamic $\mathcal{J}^{(2)}$ moments of inertia and electric quadrupole transition moments $|Q_t|$ for the three bands in ^{84}Zr studied in the present work. The bands are labeled according to Fig. 5 and according to their parity π and signature α : (π, α) . The symbols enclosed in square brackets in the top panel are extracted from the effective lifetime and mean therefore a lower limit.

cranking calculations, is observed around the band crossing region [30].

The observed quasiconstancy or very small reduction of $|Q_t|$ in the ground-state band of ^{84}Zr is a singular feature when compared with other nuclei in the $A \sim 80$ region in which the observed tendency for $|Q_t|$ is to decrease at high rotational frequency in the region in which the moment of inertia “saturates.” Examples of this contrasting behavior can be seen in several even-even nuclei in the $A=80$ region, $^{78,80}\text{Kr}$ [31–33], ^{74}Kr [34,35,30], ^{72}Se [36].

2. Negative-parity bands

The previous theoretical study [8] identified the two negative-parity bands as proton excitations and later [12] it was proposed to have a $(g_{9/2}p_{1/2})$ configuration. The proton nature of these bands was confirmed by the measured g factor [9].

Regarding the quadrupole moment, though the mean values of $|Q_t|$ for bands 2 and 3 are different above $\hbar\omega \approx 0.6$ MeV, their rather large error bars make them consistent with each other, as it should be if these bands are signature partners. The picture here is that of an essentially constant $|Q_t|$ value, an experimental result also supported by the theoretical calculations in the following section.

B. Shape evolution

In order to give a theoretical explanation regarding quadrupole moments, new calculations were performed using the cranking model with the Woods-Saxon potential similar to Ref. [8], but this time including a parametrization of the pairing interaction as a function of ω [37]. This represents an improvement compared to the previous theoretical study, in which no pairing was taken into account to calculate total Routhian surfaces; therefore, a better shape evolution prediction is expected now. In the following we will concentrate in the frequency region covered by our data and higher.

1. Ground-state band

Figure 11(a) shows both the predicted and the experimental values of $|Q_t|$ as a function of rotational frequency for the ground-state band in the frequency region above the first alignment. The experimental results are consistent with the prediction of a slow and steady decrease of $|Q_t|$ with ω . The experimental value at $\hbar\omega = 1.24$ MeV is only a lower limit. The trend of the theoretical $|Q_t|$ can be understood in Fig. 11(c), in which the shape evolution in the deformation plane (β_2, γ) is displayed. Between rotational frequencies $0.5 \leq \hbar\omega \leq 0.9$ MeV ($17 \leq I \leq 27$ in the (β_2, γ) plot), the quadrupole deformation stays essentially constant around $\beta_2 \approx 0.2$ whereas the triaxial deformation goes from $\gamma = -34^\circ$ to $\gamma = -51^\circ$. This implies a reduction of $|Q_t|$ according to Eq. (3). From there on, γ starts to approach the noncollective limit at $\gamma = -120^\circ$ while the β_2 deformation diminishes monotonically. Therefore the states become less collective. This is pretty much the expected behavior for a terminating band [38]. This means that according to the calculation the highest experimentally observed state at $I=30$

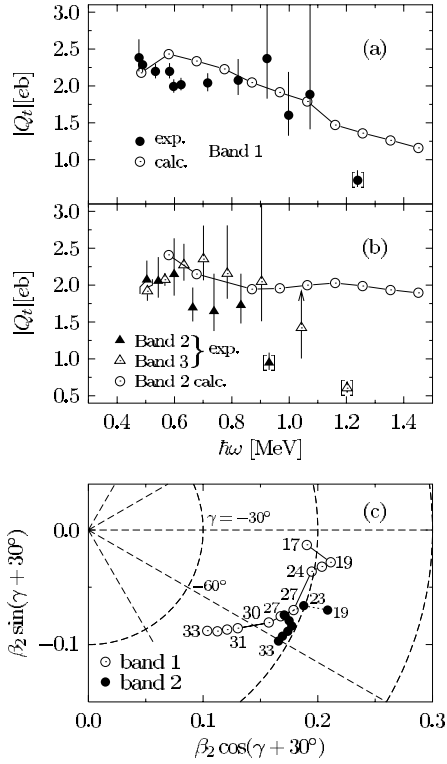


FIG. 11. Comparison between experimental and theoretically predicted quantities in rotational bands of ^{84}Zr : (a) Electric quadrupole moment in band 1 (ground-state band). (b) Experimental electric quadrupole moment in bands 2 and 3, and theoretically predicted for band 2. (c) Calculated equilibrium deformations in the (β_2, γ) plane. Numbers close to some points denote the approximate spin; larger numbers for band 1 and smaller ones for band 2.

still has collective character. Higher excited states—not yet observed—would correspond to terminating states.

2. Negative-parity bands

Figure 11(b) shows the experimental values of $|Q_t|$ for the negative-parity states together with theoretical predictions for band 2. Band 3 should present the same behavior if they are signature partners. Except for the point at $\hbar\omega=0.66$ MeV (band 2), there is agreement between the theoretical predictions and the experimental values within the region compared. The theoretical calculations for the negative-parity bands predict a similar decrease as in the positive-parity band up to $\hbar\omega \approx 0.9$ MeV. At larger frequencies the picture is quite different from that for the ground-state band as there is no essential reduction in the quadrupole moment with frequency. It is predicted that for frequencies $\hbar\omega \geq 0.9$ MeV the quadrupole moment stays constant in the same frequency range where the ground-state band terminates, as shown in the preceding section. The reason for that, according to Fig. 11(c), is the clustering of the negative-parity high-spin states in a small region with $\beta_2 \approx 0.2$ and $-54^\circ \geq \gamma \geq -60^\circ$.

The agreement between our calculations and experimental results is gratifying, particularly in the light of the somewhat surprising constancy of the experimental $|Q_t|$. The surprise appears especially if we compare the present experimental

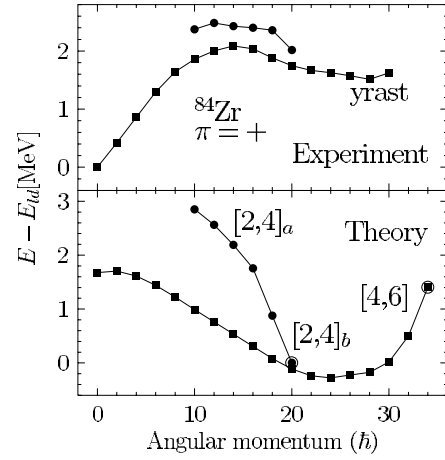


FIG. 12. Top: Energies relative to a reference rotor as a function of spin for states in the yrast band and in the new long-lived band. Bottom: Similar graphs for states calculated in the indicated configurations using the cranked Nilsson-Strutinsky approach (CNS). Note that the energies calculated in the CNS approach are not expected to be realistic below a spin of about $15\hbar$ due to neglect of pairing and, therefore, an absolute excitation energy scale cannot be established.

and theoretical results on band 1 (for which the experimental uncertainties are smaller) with those in ^{74}Kr [30], in which experiment and theory also agree but on the observation of a drastic change in shape produced by the mechanisms listed at the beginning of this section, related to the breaking of a pair. That these two, very contrasting behaviors, are present, may be again a manifestation of the rapid changes expected [39] in the collective properties when varying N and/or Z within the $A \sim 80$ region, related to the low level density in the Nilsson scheme of Fig. 1.

C. Long-lived structure

Calculations were performed within the configuration-dependent shell-correction approach using a cranked Nilsson potential (CNS) [40] in order to understand the long-lived band 4 in Fig. 5. The parameters used were previously fitted to the mass 80 region [41]. This formalism has been very successful in describing high-spin and terminating bands in ^{86}Zr [5] and other nuclei [42,1,3]. The calculated energies for the relevant configurations are shown in Fig. 12 after subtracting a rotating liquid drop reference of energy $(\hbar^2/2\mathcal{J}_{\text{rig}})I(I+1)$ with $\hbar^2/2\mathcal{J}_{\text{rig}}=0.0201$ MeV. The configurations are labeled by $[Np, Nn]$, where $Np(Nn)$ is the number of protons (neutrons) in the $g_{9/2}$ high- j orbital.

The experimental energies for the long-lived structure and the yrast band are shown in a similar way in Fig. 12 for comparison. The $[4,6]$ configuration with $\pi(N=3)^{-4}(g_{9/2})^4 \otimes \nu(N=3)^{-2}(g_{9/2})^6$ was previously proposed to represent the yrast band [43]. ($N=3$ represents the $p_{3/2}$, $f_{5/2}$, and $p_{1/2}$ orbitals which are strongly mixed.) Note that agreement below a spin of about 15 is not expected due to the neglect of pairing in the model. Above this, the theoretical and experimental curves are rather similar. The $[4,6]$ structure is predicted to terminate at the 34^+ state, in reason-

able agreement with the Woods-Saxon cranking calculations discussed earlier.

The $[2,4]$ configurations involve only two proton holes and no neutron holes in the $N=3$ orbitals. At higher spins the two proton $N=3$ holes in the $[2,4]_a$ configuration couple to the maximum possible spin of 4 leading to the fully aligned 24^+ state (not shown). By contrast, the two proton $N=3$ holes do not contribute significantly to the spin in the $[2,4]_b$ configuration because they remain in the orbitals of $p_{1/2}$ origin. Therefore this band terminates in a fully aligned 20^+ state when these holes couple to spin zero. The 16^+ and 18^+ states in this configuration, which are only slightly collective, as well as the noncollective 20^+ state, are predicted to fall significantly below those in the more collective $[2,4]_a$ configuration.

This somewhat counterintuitive situation of noncollective structures falling below the more collective ones has also been predicted for a number of other $A \sim 80$ nuclei both in this model and in the Woods-Saxon cranking model. A somewhat similar situation has been confirmed experimentally in ^{25}Mg [44]. Now the newly observed long-lived states terminating in a 20^+ level may provide experimental evidence for this phenomenon in the $A \sim 80$ nuclei. The long lifetime of the experimentally observed state and its fall in energy in Fig. 12 suggest a correspondence with the $[2,4]_b$ configuration. The difference in behavior between the predicted $[2,4]$ energies and the experimental band is similar to that between the $[4,6]$ configuration and the yrast band and probably arises from the neglect of pairing in the CNS calculations. In summary, the most likely assignment for band 4 is $[2,4]_b$, which has a dominant configuration of $\pi(g_{9/2})(p_{1/2})^{-2} \otimes \nu(g_{9/2})^6$ near its termination at $20\hbar$.

VI. CONCLUSIONS

DSAM lifetime measurements were carried out for states in the ground-state band and for the first time in highly excited states of the known negative-parity bands in ^{84}Zr . From the experimental point of view the most surprising result is that the values for spins $8 \leq I \leq 14$ in the ground-state band determined in the present work do not agree with those from several previous experiments. The reason for this disagreement seems to be in the different treatment of side-feeding time: whereas in the present work, thanks to very

good statistics, direct determination (gate from above technique) of this quantity was possible for almost all the states involved, the previous works included only simultaneous fits of both state and side-feeding time (gate from below only), providing only a correlation between both quantities and therefore leaving ambiguous the individual values.

The deduced transition quadrupole moments behave at high spins in a rather atypical way for the $A \sim 80$ mass region: the quadrupole moment in the ground-state band decreases slowly, whereas in the negative-parity bands it stays at a fairly constant value within the frequency region measured.

Hartree-Fock-Bogoliubov calculations with a Woods-Saxon potential including a frequency parametrization of pairing reproduces fairly well the experimental quadrupole moments as well for the ground-state band as for the negative-parity ones. The slow decrease of $|Q_t|$ for the ground-state band is explained as due to a small variation of the quadrupole deformation parameter β_2 while the triaxiality deformation parameter γ varies fairly monotonically from about $\gamma \approx -30^\circ$ to $\gamma \approx -60^\circ$ for the experimentally observed states. Theoretically the shape evolves further towards less deformed—not yet observed—single-particle excitations building a band termination pattern.

The theoretical calculations predict that the negative-parity bands at high spin are highly oblate ($\gamma \approx -60^\circ$) with a constant quadrupole deformation $\beta_2 = 0.2$ and evolves towards higher-spin states—not yet observed—without losing collectivity.

The long-lived structure is predicted by configuration-dependent shell-correction calculations to be a noncollective structure counterintuitively terminating at lower energies than collective structures around $I = 20^+$.

ACKNOWLEDGMENTS

This work was supported in part by the National Science Foundation under Grant Nos. PHY-9523974 and PHY-9970991 (FSU), and in part by the Department of Energy under Contract No. DE-AC03-76SR00098 (LBNL) with Lockheed Martin Energy Research Corporation, as well from Colciencias (Bogotá) under Contract No. CT-222-96. We also thank the cyclotron and GAMMASPHERE staff members at LBNL Berkeley for providing excellent research conditions.

-
- [1] R. Wadsworth, R.M. Clark, J.A. Cameron, D.B. Fossan, I.M. Hibbert, V.P. Janzen, R. Krücken, G.J. Lane, I.Y. Lee, A.O. Macchiavelli, C.M. Parry, J.M. Sears, J.F. Smith, A.V. Afanasjev, and I. Ragnarsson, Phys. Rev. Lett. **80**, 1174 (1998).
- [2] A.V. Afanasjev and I. Ragnarsson, Nucl. Phys. **A591**, 387 (1995).
- [3] C.E. Svensson, C. Baktash, G.C. Ball, J.A. Cameron, M. Devlin, J. Eberth, S. Flibotte, A. Galindo-Uribarri, D.S. Haslip, V.P. Janzen, D.R. LaFosse, I.Y. Lee, A.O. Macchiavelli, R.W. MacLeod, J.M. Nieminen, S.D. Paul, D.C. Radford, L.L. Riedinger, D. Rudolph, D.G. Sarantites, H.G. Thomas, J.C. Waddington, D. Ward, W. Weintraub, J.N. Wilson, A.V. Afanasjev, and I. Ragnarsson, Phys. Rev. Lett. **80**, 2558 (1998).
- [4] W. Nazarewicz, J. Dudek, R. Bengtsson, T. Bengtsson, and I. Ragnarsson, Nucl. Phys. **A435**, 397 (1985).
- [5] J. Döring, Y.A. Akovali, C. Baktash, F.E. Durham, C.J. Gross, P.F. Hua, G.D. Johns, M. Korolija, D.R. LaFosse, I.Y. Lee, A.O. Macchiavelli, W. Rathbun, D.G. Sarantites, D.W. Stracener, G.Z. Solomon, S.L. Tabor, A. Vander Molen, A.V. Afanasjev, and I. Ragnarsson, Phys. Rev. C **61**, 034310 (2000).
- [6] C. Plettner, H. Schnare, R. Schwengner, L. Käubler, F. Dönau, I. Ragnarsson, A.V. Afanasjev, A. Algora, G. de Angelis, A. Gadea, D.R. Napoli, J. Eberth, T. Steinhardt, O. Thelen, M. Hausmann, A. Müller, A. Jungclaus, K.P. Lieb, D.G. Jenkins,

- R. Wadsworth, A.N. Wilson, and S. Frauendorf, *Phys. Rev. C* **62**, 014313 (2000).
- [7] H.G. Price, C.J. Lister, B.J. Varley, W. Gelletly, and J.W. Olness, *Phys. Rev. Lett.* **51**, 1842 (1983).
- [8] J. Dudek, W. Nazarewicz, and N. Rowley, *Phys. Rev. C* **35**, 1489 (1987).
- [9] A.W. Mountford, J. Billowes, W. Gelletly, H.G. Price, and D.D. Warner, *Phys. Lett. B* **279**, 228 (1992).
- [10] H.-Q. Jin, C. Baktash, M.J. Brinkman, C.J. Gross, D.G. Sarantites, I.Y. Lee, B. Cederwall, F. Cristancho, J. Döring, F.E. Durham, P.-F. Hua, G.D. Johns, M. Korolija, D.R. LaFosse, E. Landulfo, A.O. Macchiavelli, W. Rathbun, J.X. Saladin, D.W. Stracener, S.L. Tabor, and T.R. Werner, *Phys. Rev. Lett.* **75**, 1471 (1995).
- [11] S. Chattopadhyay, H.C. Jain, and J.A. Sheikh, *Phys. Rev. C* **53**, 1001 (1996).
- [12] A.A. Chishti, P. Chowdhury, D.J. Blumenthal, P.J. Ennis, C.J. Lister, Ch. Winter, D. Vretenar, G. Bonsignori, and M. Savoia, *Phys. Rev. C* **48**, 2607 (1993).
- [13] T.D. Johnson, A. Aprahamian, C.J. Lister, D.J. Blumenthal, B. Crowell, P. Chowdhury, P. Fallon, and A.O. Macchiavelli, *Phys. Rev. C* **55**, 1108 (1997).
- [14] J. Döring, R.A. Kaye, A. Aprahamian, M.W. Cooper, J. Daly, C.N. Davids, R.C. de Haan, J. Görres, S.R. Leshner, J.J. Ressler, D. Seweryniak, E.J. Stech, A. Susalla, S.L. Tabor, J. Uusitalo, W.B. Walters, and M. Wiescher, *Phys. Rev. C* **67**, 014315 (2003).
- [15] C. Teich, A. Jungclaus, V. Fischer, D. Kast, K.P. Lieb, C. Link, C. Ender, T. Härtlein, F. Köck, D. Schwalm, J. Billowes, J. Eberth, and H.G. Thomas, *Phys. Rev. C* **59**, 1943 (1999).
- [16] I.Y. Lee, *Nucl. Phys.* **A520**, 641c (1990).
- [17] D.G. Sarantites, P.-F. Hua, M. Devlin, L.G. Sobotka, J. Elson, J.T. Hood, D.R. LaFosse, J.E. Sarantites, and M.R. Maier, *Nucl. Instrum. Methods Phys. Res. A* **381**, 418 (1996).
- [18] E.F. Moore, P.D. Cottle, C.J. Gross, D.M. Headly, U.J. Hüttmeier, S.L. Tabor, and W. Nazarewicz, *Phys. Rev. C* **38**, 696 (1988).
- [19] M. Wiedeking, R.A. Kaye, G.Z. Solomon, S.L. Tabor, J. Döring, G.D. Johns, F. Cristancho, M. Devlin, F. Lerma, D.G. Sarantites, I.Y. Lee, and A.O. Macchiavelli, *Phys. Rev. C* **62**, 024316 (2000).
- [20] R.A. Kaye, C.T. Rastovski, S.L. Tabor, J. Döring, M. Devlin, G.D. Johns, I.Y. Lee, F. Lerma, A.O. Macchiavelli, D.G. Sarantites, and G.Z. Solomon, *Phys. Rev. C* **66**, 054305 (2002).
- [21] R. Lortz, O. Iordanov, E. Galindo, A. Jungclaus, D. Kast, K.P. Lieb, C. Teich, F. Cristancho, Ch. Ender, T. Härtlein, F. Köck, and D. Schwalm, *Eur. Phys. J. A* **6**, 257 (1999).
- [22] F. Cristancho, K.P. Lieb, J. Heese, C.J. Gross, W. Fieber, Th. Osipowicz, S. Ulbig, K. Bharuth-Ram, S. Skoda, J. Eberth, A. Dewald, and P. von Brentano, *Nucl. Phys.* **A501**, 118 (1989).
- [23] J. F. Ziegler, J. P. Biersack, and U. Littmark, *The Stopping and Range of Ions in Matter* (Pergamon, New York, 1985).
- [24] J. F. Ziegler, www.srim.org (SRIM version 2000. 40).
- [25] K. P. Lieb, in *Experimental Techniques in Nuclear Physics*, edited by Dorin N. Poenaru and Walter Greiner (Walter de Gruyter, Berlin, 1997).
- [26] S.L. Tabor, J. Döring, J.W. Holcomb, G.D. Johns, T.D. Johnson, T.J. Petters, M.A. Riley, and P.C. Womble, *Phys. Rev. C* **49**, 730 (1994).
- [27] F. Cristancho and K.P. Lieb, *Nucl. Phys.* **A524**, 518 (1991).
- [28] E. Galindo and F. Cristancho, in *Instrumentation in Elementary Particle Physics*, edited by G. Herrera Corral and M. Sosa Aquino, AIP Conf. Proc. 422 (AIP, Woodbury, 1998), p. 387.
- [29] W. Nazarewicz and I. Ragnarsson, in *Handbook of Nuclear Properties*, edited by Dorin Poenaru and Walter Greiner (Clarendon, Oxford, 1996).
- [30] A. Algora, G. de Angelis, F. Brandolini, R. Wyss, A. Gadea, E. Farnea, W. Gelletly, S. Lunardi, D. Bazzacco, C. Fahlander, A. Aprahamian, F. Becker, P.G. Bizzeti, A. Bizzeti-Sona, D. de Acuña, M. De Poli, J. Eberth, D. Foltescu, S.M. Lenzi, T. Martinez, D.R. Napoli, P. Pavan, C.M. Petrache, C. Rossi Alvarez, D. Rudolph, B. Rubio, S. Skoda, P. Spolaore, R. Menegazzo, H.G. Thomas, and C.A. Ur, *Phys. Rev. C* **61**, 031303(R) (2000).
- [31] P.K. Joshi, H.C. Jain, R. Palit, G. Mukherjee, and S. Nagaraj, *Nucl. Phys.* **A700**, 59 (2002).
- [32] L. Funke, J. Döring, F. Dubbers, P. Kemnitz, E. Will, G. Winter, V.G. Kiptilij, M.F. Kudojarov, I.Kh. Lemberg, A.A. Pateranak, A.S. Mishin, L. Hildingsson, A. Johnson, and Th. Lindblad, *Nucl. Phys.* **A355**, 228 (1981).
- [33] G. Mukherjee, H.C. Jain, R. Palit, P.K. Joshi, S.D. Paul, and S. Nagaraj, *Phys. Rev. C* **64**, 034316 (2001).
- [34] S.L. Tabor, P.D. Cottle, J.W. Holcomb, T.D. Johnson, P.C. Womble, S.G. Buccino, and F.E. Durham, *Phys. Rev. C* **41**, 2658 (1990).
- [35] J. Heese, D.J. Blumenthal, A.A. Chishti, P. Chowdhury, B. Crowell, P.J. Ennis, C.J. Lister, and Ch. Winter, *Phys. Rev. C* **43**, R921 (1991).
- [36] R. Palit, H.C. Jain, P.K. Joshi, J.A. Sheikh, and Y. Sun, *Phys. Rev. C* **63**, 024313 (2001).
- [37] U.J. Hüttmeier, C.J. Gross, D.M. Headly, E.F. Moore, S.L. Tabor, T.M. Cormier, P.M. Stwertka, and W. Nazarewicz, *Phys. Rev. C* **37**, 118 (1988).
- [38] A.V. Afanasjev, D.B. Fossan, G.J. Lane, and I. Ragnarsson, *Phys. Rep.* **322**, 1 (1999).
- [39] W. Nazarewicz, in *High Spin Physics and Gamma Soft Nuclei*, edited by J. X. Saladin, R. A. Sorensen, and C. M. Vincent (World Scientific, Singapore, 1991), p. 406.
- [40] T. Bengtsson and I. Ragnarsson, *Nucl. Phys.* **A436**, 14 (1985).
- [41] D. Galeriu, D. Bucurescu, and M. Ivaşcu, *J. Phys. G* **12**, 329 (1986).
- [42] I. Ragnarsson, V.P. Janzen, D.B. Fossan, N.C. Schmeing, and R. Wadsworth, *Phys. Rev. Lett.* **74**, 3935 (1995).
- [43] I. Ragnarsson and T. Bengtsson, in *Nuclear Structure of the Zirconium Region*, edited by J. Eberth, R. A. Meyer, and K. Sistemich (Springer-Verlag, Berlin, 1988), p. 193.
- [44] D.M. Headly, R.K. Sheline, S.L. Tabor, U.J. Hüttmeier, C.J. Gross, E.F. Moore, B.H. Wildenthal, H.R. Weller, R.M. Whitton, and I. Ragnarsson, *Phys. Lett. B* **198**, 433 (1987).